Dynamical conductivity of soliton lattice and polaron lattice in the continuum model of polyacetylene

Han-Yong Choi and E. J. Mele
Department of Physics, University of Pennsylvania, Philadelphia, Pennsylvania 19104-6396
(Received 28 April 1986)

The dynamical conductivity due to phonons around the soliton lattice and around a polaron lattice, and the creation energy of these two structural configurations were calculated in a continuum model of polyacetylene. The crossover from the soliton lattice to the polaronlike distortion proposed by Kivelson and Heeger to explain the abrupt onset of the magnetic susceptibility around 5% doping is not found in a strictly one-dimensional calculation. The harmonic lattice fluctuations around the static equilibrium configurations were obtained and used to calculate and compare the absorption spectra for the various defect configurations.

I. INTRODUCTION

Since Su, Schrieffer, and Heeger[1] proposed the soliton model of polyacetylene, a number of experimental studies and theoretical calculations have been carried out to support this model. Theoretical predictions on the soliton hopping mechanisms for the electric conductivity at very light doping level, on the vibrational excitations of charged solitons and on the effect of dilute doping on optical absorption spectra have been confirmed by various experiments. Undoped polyacetylene has a half-filled π band and therefore is unstable against Peierl's transition to become a dimerized semiconductor. Upon doping, the dc electric conductivity increases sharply by 11 orders of magnitude at 1–2% doping level. However, up to 5% doping density the strength of the Pauli spin contribution to the magnetic susceptibility is much smaller than one would expect in a metal of similar conductivity. This anomalous low-χ, high-σ behavior led to a suggestion that the conduction in this regime is by unpinned charged solitons. Interestingly, this anomalously low magnetic susceptibility is abruptly increased around 5% doping level.[2] To explain this observation, Kivelson and Heeger proposed recently[3] that this onset of magnetic susceptibility is due to the crossover from a soliton lattice[4] to a metallic state consisting of a regular array of polaronlike distortions.

We have carried out calculations investigating the creation energy and dynamical conductivity for static configurations such as the dimerized lattice, the soliton lattice, and a polaronlike lattice in the model of Takayama, Lin Liu, and Maki[5] (TLM), to see if numerical calculations support this idea. We found that there is no crossover between the soliton lattice and the polaronlike lattice in the strict TLM model. Moreover, at high density the polaronlike lattice is unstable against the *undimerized* lattice. We checked the possibility that the pinning potential from an ordered lattice of ionized dopants might favor the polaronlike lattice over the undimerized one, but we found that this does not occur. Having obtained the static equilibrium configurations corresponding to the soliton lattice and the polaronlike lattice, we have also analyzed the phonon modes arising from small harmonic fluctuations around these static configurations. Normal mode analyses around the dimerized configuration, single soliton, and single polaron were carried out by several groups.[6–8] Analysis around the soliton lattice was done by us and will be reported in a separate paper.[9] We have also calculated the dynamical conductivity due to these phonon spectra. Similar calculations around a soliton and a polaron have been reported by Mele and Hicks[10] and Ito and Ono.[11] The dynamical conductivity due to phonons around the soliton lattice and polaronlike lattice was obtained following our previous work by introducing the internal vibrational degrees of freedom of each primitive cell [$(CH)_{-x}$ unit]. These calculations were done both at the low-doping density (1%) and at slightly above the experimentally observed transition density (−7%) and compared with experiments. Surprisingly, we find that in the polaronlike lattice at high density, the ir conductivity is very small, which is not consistent with experiment. An alternative model for the high-density metallic state will be discussed.

In Sec. II we will first review the general formulation for calculating the dynamical conductivity due to phonons around the static equilibrium configuration along with the method for incorporating the internal vibrational degrees of freedom of a $(CH)_{-x}$ chain. Explicit calculation and the results of absorption spectra will be discussed in Sec. III.

II. FORMULATION

The Hamiltonian for $(CH)_{-x}$ is transformed, after taking the continuum limit,[5] to

$$H=\frac{1}{\pi v_F\lambda}\int dx\left[\Delta^2(x,t)+\frac{1}{\omega_Q^2}\dot{\Delta}^2(x,t)\right]+\sum_{\text{spin}}\int dx\,\Psi^+(x,t)\left[-iv_F\sigma_3\frac{d}{dx}+\sigma_1\Delta(x,t)\right]\Psi(x,t)\ , \tag{1}$$

where λ is dimensionless electron-phonon coupling constant ($=0.38$), v_F the Fermi velocity, $\Delta(x,t)$ is the order parameter representing the staggered lattice-displacement field, ω_Q the bare optical-phonon frequency, and $\Psi(x,t)$ is the electron wave function in spinor form, the first and second component of which represent the right- and left-going waves, respectively, and σ_1 and σ_3 are the Pauli matrices. We have the following equations after taking the functional derivative of Eq. (1) with respect to $\delta\Psi^+$ and $\delta\Delta$:

$$\left[-iv_F\sigma_3\frac{d}{dx}+\sigma_1\Delta(x)\right]\Psi_k(x)=E_k\Psi_k(x)\ , \tag{2}$$

$$\frac{2}{\pi v_F\lambda}\Delta(x)+2\sum_k^{\text{occ}}\Psi_k^+\sigma_1\Psi_k(x)=0\ . \tag{3}$$

Equation (3) is the self-consistency relation which guarantees that our system is at a local extremum on the energy surface. Equation (2) is the eigenvalue problem, from which we obtain the one-electron energy spectrum. Then the total energy is just given by

$$E_{\text{tot}}=-2\sum_k{}'E_k+\frac{1}{\pi v_F\lambda}\int dx\ \Delta^2(x)\ . \tag{4}$$

The factor of 2 comes from spin degeneracy, and the prime means that the sum over k runs up to Fermi level, which changes as we put extra electrons (doping) into the system, so that E_{tot} is a function of the dopant density. The requirement that E_{tot} should be stationary with respect to the small variation of $\Delta(x)$ just gives the self-consistency condition [Eq. (3)]. Calculations of E_{tot} with Eq. (4) as a function of doping density for different structural distortions were carried out, and the creation energy per excess electron for each configuration was obtained as follows:

$$E_{\text{cre}}=[E_{\text{tot}}(\Delta(x),N)-E_0]/N\ , \tag{5}$$

where E_0 is the total energy of the dimerized configuration without doping and N is the number of excess electrons. E_{cre} for different configurations is plotted in Fig. (1), where curve a represents the creation energy per charge for the soliton lattice calculated by Horovitz,[4] curve b for a polaronlike lattice, curve c for an undimerized lattice, and curve d for a dimerized one.

It is interesting to note that although the soliton lattice is favored at all densities in this model, the energy per particle as the undimerized lattice (curve c), polaronlike lattice (curve b), and soliton lattice (curve a) converges above an 8% doping level. As Kivelson has noted, this implies that small perturbation outside the TLM model may reorder these energies. Since we are particularly interested in which polaronlike lattice might be favored over the soliton lattice, we have also considered the influence of a screened Coulomb pinning potential (due to an ordered impurity lattice) on these energies. We have found that for reasonable estimates of the pinning potential the soliton lattice remains energetically favored over the polaron lattice at all densities considered. While this implies that the polaron lattice is unstable against the soliton lattice at all densities even in a more realistic model, we

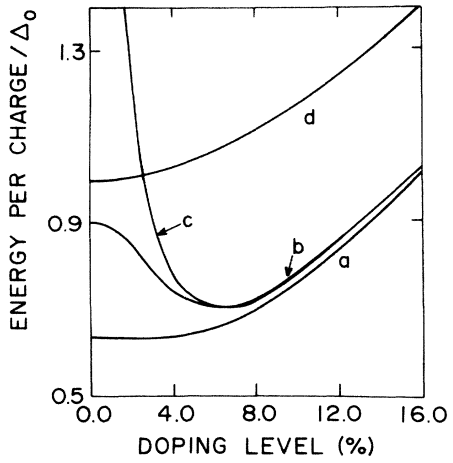

FIG. 1. Creation energy per charge for several structural configurations. Curve a refers to the creation energy for the soliton lattice, curve b is for the polaronlike lattice, curve c is for the undimerized lattice, and curve d is for the dimerized lattice.

should note that the relaxation from the polaron lattice to soliton lattice proceeds along a zone-boundary phonon of the polaron lattice. This means that like the soliton lattice, the polaron lattice can describe an equilibrium field configuration, if we constrain the system to be translationally invariant with a primitive translation vector $R=a/c$, where c is the dopant concentration and a is the c-c bond length. With the constraint, the zone-center modes all have $\omega^2\geq 0$, while one obtains an unstable branch at the Brillouin-zone boundary which describes the relaxation to the energetically favored, lower symmetry, soliton lattice. Since the zone-center modes are important for the infrared conductivity, we will use this constraint on the translational invariance of the system in order to explore properties of the polaron lattice. A detailed discussion on the calculation of the dynamical conductivity was given by Ito and Ono,[11] so we will not go through this theory in detail. The idea, however, is to calculate the electron current density in the presence of a small perturbation $\delta\Delta(x,t)$. The current density in the TLM model is given by

$$\begin{aligned} j(x,t)&=-ev_F\sum_{n,s}{}'\Psi_n^+(x,t)\sigma_3\Psi_n(x,t)\\ &=-ev_F\sum_{n,s}{}'[\delta\Psi_n^+(x,t)\sigma_3\Psi_n^{(0)}(x)\\ &\quad+\Psi_n^{(0)+}(x)\sigma_3\delta\Psi_n(x,t)]\ , \end{aligned} \tag{6}$$

where $\Psi_n^{(0)}(x)$ is the eigenfunction of the unperturbed Hamiltonian equation (2) and we have used the fact that no phonon-assisted current exists in the ground state [we dropped $j^{(0)}(x)=\Psi^{(0)+}(x)\sigma_3\Psi^{(0)}(x)$]. The deviation of the wave function due to $\delta\Delta$ is (we will drop superscript 0 for convenience):

$$\delta\Psi_n(x,\omega)=\sum_m\frac{\Psi_m(x)}{E_n-E_m+\omega}\langle m\mid\sigma_1\delta\Delta(\omega)\mid n\rangle\ . \tag{7}$$

We Fourier-transform Eq. (6) and substitute into Eq. (7), to get an expression for $j(x,\omega)$. Since we are interested in the response of our system to a long-wavelength external field, we extract the $q=0$ portion of the induced current by an integration on x. Then

$$j(\omega)=-\frac{ev_F}{L}\sum_{n,s}{}'\sum_m\left[\frac{\langle n\mid\sigma_1\delta\Delta(\omega)\mid m\rangle\langle m\mid\sigma_3\mid n\rangle}{E_n-E_m+\omega}+\frac{\langle m\mid\sigma_1\delta\Delta(\omega)\mid n\rangle\langle n\mid\sigma_3\mid m\rangle}{E_n-E_m-\omega}\right], \tag{8}$$

and thus the real part of infrared conductivity is given by

$$\mathrm{Re}\sigma(\omega)=-\frac{(ev_Fg)^2}{2\omega^2LA}\mid M_\gamma(\omega)\mid^2\pi\delta(\omega-\omega_\gamma)\ , \tag{9}$$

$$M_\gamma(\omega)=\sum_{n,s}{}'\sum_m\left[\frac{\langle n\mid\sigma_1u_\gamma\mid m\rangle\langle m\mid\sigma_3\mid n\rangle}{E_n-E_m+\omega}+\frac{\langle m\mid\sigma_1u_\gamma\mid n\rangle\langle n\mid\sigma_3\mid m\rangle}{E_n-E_m-\omega}\right]$$
$$=-\sum_{n,s}{}'\sum_m\frac{4\omega\langle n\mid\sigma_1u_\gamma\mid m\rangle\langle m\mid\sigma_3\mid n\rangle}{(E_n-E_m)^2-\omega^2}\ . \tag{10}$$

We drop ω^2 in $(E_n-E_m)^2-\omega^2$ (adiabatic approximation), to obtain

$$\mathrm{Re}\sigma(\omega)=\frac{(2ev_Fg)^2}{LA}\left|\sum_n{}'\sum_m\frac{\langle n\mid\sigma_1u_\gamma\mid m\rangle\langle m\mid\sigma_3\mid n\rangle}{(E_n-E_m)^2}\right|^2\times2\pi\delta(\omega-\omega_\gamma)\ , \tag{11}$$

where L is the length and A is the cross section per chain in the polyacetylene bundle which we take to be 10.5Å^2, and $u_\gamma(\omega)$ is the phonon mode corresponding to ω_γ.

In order to take into consideration the internal degree of vibrational freedom of a $(CH)_{-x}$ unit, we consider the Hamiltonian with several $\Delta_n(x)$.[12] Then the Hamiltonian describing this system is generalized to

$$H=\sum_{n=1}^{N}\frac{1}{\pi v_F\lambda_n}\int dx\left[\Delta_n^2(x,t)+\frac{1}{\omega_{nQ}^2}\dot{\Delta}_n^2(x,t)\right]+\sum\int dx\,\Psi^+(x,t)\left[-iv_F\sigma_3\frac{d}{dx}+\sigma_1\Delta(x)\right]\Psi(x,t)\ , \tag{12}$$

with

$$\Delta(x,t)=\sum_n\Delta_n(x,t)$$

and

$$\lambda=\sum_n\lambda_n\ .$$

We expand H up to second order in $\delta\Delta_n$, to have from Hamiltonian's equations of motion

$$-\frac{1}{\omega_{nQ}^2}\delta\ddot{\Delta}_n=\delta\Delta_n(x,t)+\pi v_F\lambda_n\int K(x,x')\delta\Delta(x')dx'\ , \tag{13}$$

where K is the dynamical matrix which can be represented in terms of normal modes as

$$\pi v_F\lambda K(x,x')=\sum_\alpha u_\alpha(x)\left[-1+\frac{\omega_\alpha^2}{\omega_Q^2}\right]u_\alpha^*(x')\ , \tag{14}$$

where ω_α is the αth normal frequency and $u_\alpha(x)$ is the corresponding normal mode. We substitute Eq. (14) into Eq. (13), to obtain

$$\frac{\omega^2}{\omega_{nQ}^2}\delta\Delta_n(x)=\delta\Delta_n(x)+\lambda_n/\lambda\int dx'\delta\Delta(x')\sum_{\alpha'}u_{\alpha'}(x)\left[\frac{\omega_{\alpha'}^2}{\omega_Q^2}-1\right]u_{\alpha'}^*(x')\ . \tag{15}$$

We expand $\delta\Delta_n(x)$ in terms of $u_\alpha(x)$ as

$$\delta\Delta_n(x)=\sum_\alpha A_{n\alpha}u_\alpha(x)$$

and use orthogonality

$$\int u_\alpha^*(x)u_{\alpha'}(x)dx=\delta_{\alpha\alpha'}$$

to get

$$(\omega^2-\omega_{nQ}^2)A_{n\alpha}=\frac{\lambda_n\omega_{nQ}^2}{\lambda\omega_Q^2}(\omega_\alpha^2-\omega_Q^2)\sum_{n'}A_{n'\alpha}\ .$$

If we introduce electron-phonon coupling constant g, which is given by $g_n^2=\pi v_F\lambda_n\omega_{nQ}^2$, then

$$(\lambda_n\omega_{nQ}^2/\lambda\omega_Q^2)^{1/2}=g_n/g\ .$$

We can make the matrix symmetric by transforming $A_{n\alpha}$ to $B_{n\alpha}$ with

$$B_{n\alpha}=\frac{A_n\alpha}{(\lambda_n\omega_{nQ}^2/\lambda\omega_Q^2)^{1/2}}=\frac{A_{n\alpha}}{(g_n/g)}\ .$$

Then, we finally have

$$(\omega^2-\omega_{nQ}^2)B_{n\alpha}=\sum_{n'}(g_n/g)(g_{n'}/g)(\omega_\alpha^2-\omega_Q^2)B_{n'\alpha}\ . \tag{16}$$

For this to have a nontrivial solution

$$\det[(\omega_{nQ}^2-\omega^2)\delta_{n,n'}+(g_n/g)(g_{n'}/g)(\omega_\alpha^2-\omega_Q^2)]=0\ . \tag{17}$$

Given three bare optical frequencies ω_{nQ} and coupling constants λ_n, listed in Table I,[13] we can solve Eq. (17) for

TABLE I. Bare optical frequencies and coupling constants for the continuum model of polyacetylene.

n	ω_{nQ} (cm^{-1})	λ_n/λ
1	1234	0.07
2	1309	0.02
3	2040	0.91

particular normal frequency ω_α to get three eigenvalues $\omega_{i\alpha}$ (the new normal frequencies) and their corresponding eigenvectors which incorporate the internal structural degree of freedom $B_{in\alpha}$. Then the contribution to dynamical conductivity from this internal vibrational mode with normal frequency $\omega_{i\alpha}$ is given by

$$\mathrm{Re}\sigma(\omega)=\sum_{i,\alpha}\frac{(2ev_Fg)^2}{LA}2\pi\delta(\omega-\omega_{i\alpha})\,|P_\alpha|^2 \times\left|\sum_{n=1}^{3}\left[\frac{g_n}{g}\right]B_{in\alpha}\right|^2, \tag{18}$$

where

$$P_\alpha=\sum_{l,m}\frac{\langle l|\sigma_1 u_\alpha|m\rangle\langle m|\sigma_3|l\rangle}{(E_l-E_m)^2} =\int dx\,u_\alpha(x)j_d(x)\,, \tag{19}$$

and $j_d(x)$ is the dynamical charge.

We can note that for a given α the set of modes ($i=1$ to 3) have a common spatial part P_α which involves $u_\alpha(x)$ so that they are modulated only by the sum over $B_{in\alpha}$. Since all λ_n's are positive definite, the strongest infrared active mode in each symmetry allowed subspace are always the lowest branches in which the B's are all in phase.

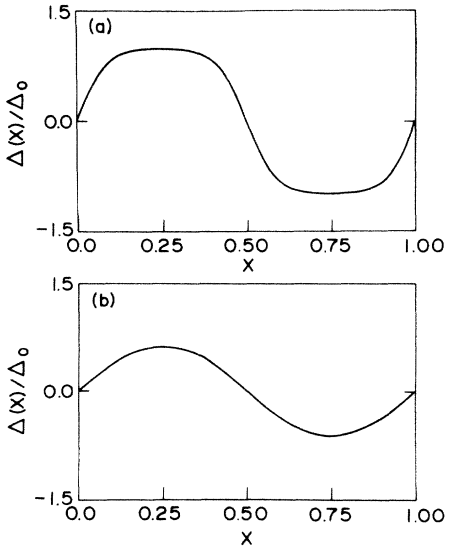

FIG. 2. Order parameter for the soliton lattice at (a) 2.37% and (b) 6.85%.

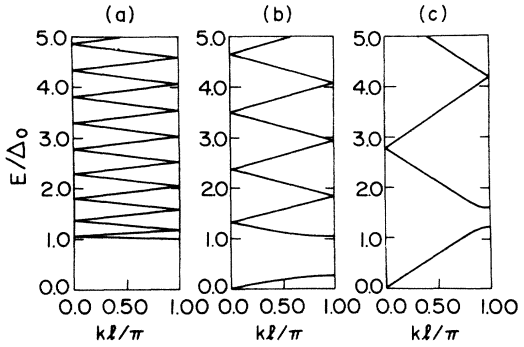

FIG. 3. The electronic bands for the soliton lattice at (a) 2.37%, (b) 5.14%, and (c) 12.3%.

III. RESULTS

The equilibrium static displacement fields are plotted for the soliton lattice at a 2.4% doping level in Fig. 2(a), and at a 6.9% doping level in Fig. 2(b). In Fig. 3, we plot the corresponding electronic energy bands. It is interesting to note that both the amplitude of the static displacement field and the size of the gap in the electronic spectrum decrease monotonically as the dopant density increases in the continuum model. For the polaronlike distortion, the equilibrium static displacement fields are shown in Fig. 4 for a 1% concentration of polarons. At this density this is an equilibrium displacement field for the period shown. In Fig. 4 it is compared with the $\mathrm{sech}^2(x)$ shape expected for an isolated polaron. Comparing the two curves, we see that even at 1% concentration the structural distortion does not closely resemble that constructed from a superposition of isolated polarons at this density. Instead there is a tendency for the trapped charges to delocalize, increasing the spatial extent and decreasing the amplitude of the structural distortion away from the uniformly dimerized lattice. The electronic energy bands for this density are given in Fig. 5. It shows narrow polaron band split away from the conduction states with $E(k)>\Delta_0$. At still higher density, the equili-

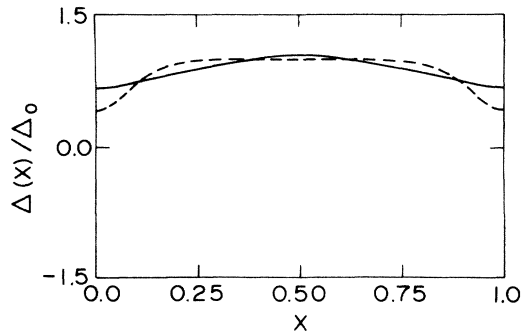

FIG. 4. Order parameter for the polaronlike lattice at 1.03%. The solid line represents the order parameter after relaxation, and the dashed line represents the superposition of the isolated polarons.

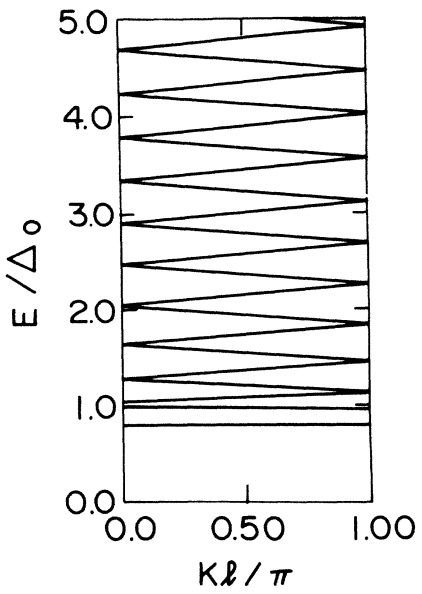

FIG. 5. The electron bands for the polaronlike lattice at 1.03%.

brium amplitude of the distortion decreases significantly for the polaronlike lattice, so that the system is well approximated by the undimerized lattice for density $\rho \geq 6\%$. This can be seen from the total-energy data plotted in Fig. 1, where the polaron lattice and the undimerized lattice energies converge for $\rho \geq 6\%$.

Using the expression for the phonon-assisted conductivity given by Eq. (18), we calculate the absorption spectra. The infrared conductivity can be experimentally probed by the measurement of absorption coefficient $\alpha(\omega)$ given by

$$\alpha(\omega)=\frac{4\pi}{c}\mathrm{Re}\sigma(\omega)$$
$$=\frac{4\pi}{c}\sum_{i,\alpha}\frac{(2ev_F g)^2}{LA}|P_\alpha|^2\left|\sum_{n=1}^{3}\left[\frac{g_n}{g}\right]B_{in\alpha}\right|^2$$
$$\times 2\pi\delta(\omega-\omega_{i\alpha}) , \quad (20)$$

where P_α is given by Eq. (19). The three bare optical frequencies ω_{nQ} and coupling constants λ_n for continuum model for trans-$(CH)_x$ are given in Table I. In Tables II and III we list the normal mode frequencies ω_α for the one-component theory for soliton lattice and polaronlike lattice at two doping densities, respectively, along with the overall parity of the mode. The overall parity of a normal mode is obtained by multiplying the parity of the envelope function describing the normal mode and the parity of the internal ion displacement describing an ir-allowed mode. The field variable $\Delta(x)$ describing the envelope function of the staggered displacement field is an odd parity field for the soliton lattice but an even parity field for the polaronlike lattice. Only the normal modes which have odd overall parity are the modes which have the correct symmetry to induce a net oscillating dipole moment in the system. The envelope function describing the infrared-active mode has the opposite parity to the static displacement field $\Delta(x)$. The simplest example of this is the envelope function for the Goldstone mode $u_G(x)=d\Delta(x)/dx$ which clearly has the opposite parity to $\Delta(x)$.

As can be seen in Eqs. (19) and (20), the oscillator strength in a particular infrared active mode is given by the square of the overlap between $j_d(x)$ and normal mode $u_\alpha(x)$, modulated by the square of the dot product of $\{B_{in\alpha}\}$ and $\{g_n\}$. It is interesting to note that $j_d(x)$ looks very similar to the Goldstone mode (the mode that has zero frequency due to the symmetry breaking), so that almost all oscillator strength is found in the Goldstone mode. At higher density, or for the lattice distortion with less localized charge distribution, the excess charge density tends to delocalize so that we expect more oscillator strength to leak into the higher-lying internal modes from the localized vibrational modes. Strickly speaking, these are not localized because the soliton lattice or polaronlike lattice is periodic, but what we mean here by "localized" is that the vibrations around defect sites are much larger than those of interdefects region. The charge also tends to be more delocalized for the isolated polaron than for the isolated soliton, so that we expect an enhanced ir activity for the internal modes of the polaron compared to those of the soliton lattice. The numerical calculations demonstrate this trend. Figure 6 contains the absorption spectra calculated for both the soliton lattice and the polaronlike lattice at low density, and Fig. 7 contains the spectra at high density. The polaronlike lattice has more fine struc-

TABLE II. Normal-mode frequency for soliton lattice in one-component theory.

α \ Density	2.37%		6.85%	
	$\omega_\alpha^2/\omega_0^2$	Overall parity	$\omega_\alpha^2/\omega_0^2$	Overall parity
1	0.000	−	0.377	−
2	0.019	+	0.507	+
3	0.721	+	0.518	+
4	0.777	+	1.094	+
5	0.964	+	1.136	+
6	1.013	−	1.570	+
7	1.035	+	1.584	−
8	1.547	+	1.922	+
9	1.548	+	1.926	+

TABLE III. Normal-mode frequency for polaron lattice.

Density / α	1.03% $\omega_\alpha^2/\omega_0^2$	1.03% Overall parity	6.16% $\omega_\alpha^2/\omega_0^2$	6.16% Overall parity
1	0.000	−	0.320	+
2	0.691	+	0.875	−
3	0.880	+	0.959	+
4	1.153	+	1.764	−
5	1.168	−	1.767	+
6	1.479	+	2.327	−
7	1.491	−	2.328	+
8	1.627	+		
9	1.634	−		
10	1.695	+		
11	1.697	−		
12	1.784	+		

ture in the absorption spectra than the soliton lattice and this comes from the fact that the excess charges are more delocalized as can be seen from the order parameter $\Delta(x)$ in Fig. 4. The interesting result about the soliton lattice is that we have found three localized modes in the one-component calculation, two of which are ir active [T and A^-, T stands for translational mode (or Goldstone mode) A^- stands for soliton-width oscillation mode]. In the three-component model for Tables IV and V, the T mode contributes to the three large peaks at 0, 1280, and 1350 cm^{-1} and the A^- mode to two additional small peaks at 1080 and 1460 cm^{-1} (a small peak at 1300 cm^{-1} from A^- is imbedded in the large peaks from the T mode and is invisible). These small peaks from the A^- mode were usually thought to be characteristic of polaronlike distortion.[8,14] We should point out that there is a controversy about this; the third bound mode (A^- mode) was first observed in the one-component calculation by Ito *et al.*, who carried out the calculations for a very small coupling constant for which the continuum model should be most accurate. In our calculation we have developed a general scheme[9] which allows an accurate calculation of the nonlocal kernel in the continuum model for an arbitrary coupling constant. Here we take $\lambda=0.38$, which is representative of the situation for trans-$(CH)_x$. We believe that the previous calculation of Hicks and Blaisdell, who obtained two bound modes, results from a slightly less accurate treatment of the ultraviolet cutoff in the momentum sum in the calculation of the kernel. We should note that the more recent calculations of Hicks and Gammel[15] introduce a lattice cutoff in this theory and also recover the third bound mode. For polaronlike lattice we have found six localized vibrational modes, two of which are ir active (T and A^- modes). This explains why the ir absorption spectrum for the polaronlike distortion looks similar to that for the soliton lattice. But for the polaronlike lattice the higher-lying modes are more ir active than for the soliton lattice, which causes more pronounced fine structure in the absorption spectra.

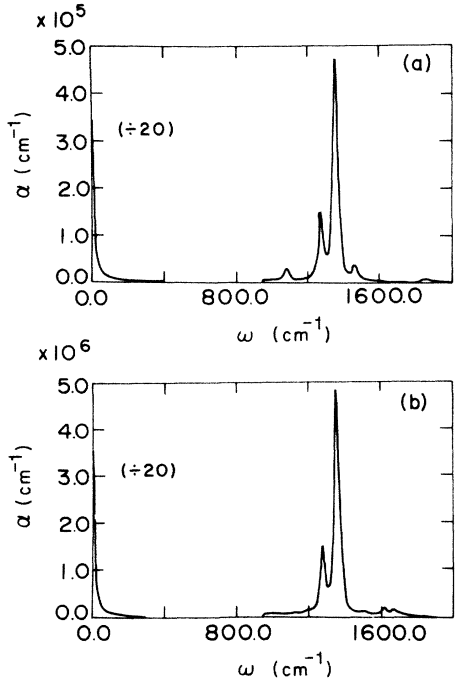

FIG. 6. Absorption spectra for the soliton lattice and the polaronlike lattice at low dopant density. (a) refers to the soliton lattice at 2.37%, and (b) to the polaronlike lattice at 1.03%.

There is one important additional effect which we have to take into consideration for the polaronlike lattice. Because the polaronlike lattice has a half-filled band, we have to consider intraband transitions which will also contribute to the absorption spectra around $\omega=0$. In the presence of impurity (dopant) pinning, the Goldstone mode will be shifted to have a finite frequency, but the (damped) intraband transition will still peak around $\omega=0$. This intraband transition is not allowed in the soliton lattice because the soliton band is completely filled. We did not incorporate this intraband transition in our calculation. We argue that this will not be important at very low density because the polaron band is very flat leading to a large effective mass for the free carriers. At high density, the intraband term also makes a negligible contribution, which can be understood in the following way. The high-density polaronlike distortion is well approximated

TABLE IV. Ir-active-mode frequency for soliton lattice in multicomponent theory.

α	$\omega_\alpha^2/\omega_0^2$	i	$\omega_{i\alpha}$ (cm^{-1})
	Density: 2.37%		
1	0.0	1	0
		2	1279
		3	1354
6	1.013	1	1080
		2	1293
		3	1464
	Density: 6.85%		
1	0.377	1	708
		2	1283
		3	1373
7	1.584	1	1191
		2	1301
		3	1651

by the undimerized lattice, for which the eigenfunction in spinor representation is just a plane wave for one component and vanishes for the other component, so that $\langle l \mid \sigma_1 \mid m \rangle$ in Eq. (19) will vanish in the high-density limit. At intermediate density it may be important to include the intraband contribution to the polarizability. It must also be included in the calculation of zone-boundary modes in the present model, where the intraband transitions destablize a branch of the phonon spectrum of a polaron lattice at zone boundary.

TABLE V. Ir-active-mode frequency for polaron lattice in multicomponent theory.

α	$\omega_\alpha^2/\omega_0^2$	i	$\omega_{i\alpha}$ (cm^{-1})
	Density: 1.03%		
1	0.0	1	0
		2	1279
		3	1354
5	1.168	1	1125
		2	1295
		3	1507
7	1.491	1	1181
		2	1300
		3	1616
9	1.634	1	1195
		2	1301
		3	1669
11	1.697	1	1200
		2	1302
		3	1693
	Density: 6.16%		
2	0.875	1	1027
		2	1291
		3	1434
4	1.764	1	1205
		2	1303
		3	1719
6	2.327	1	1228
		2	1307
		3	1930

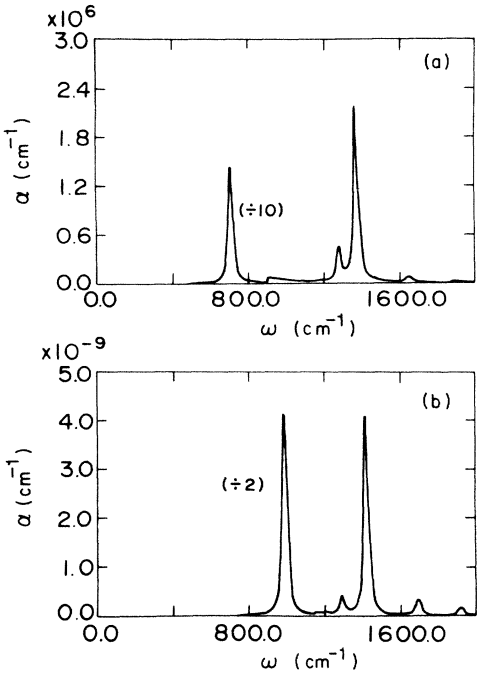

FIG. 7. Absorption spectra for the soliton lattice and the polaronlike lattice at high dopant density. (a) refers to the soliton lattice at 6.85%, and (b) to the polaronlike lattice at 6.16%.

An interesting point to be noticed in the calculated ir spectra shown in Fig. 8 is the doping density dependence of the integrated oscillator strength $[= \int d\omega \alpha(\omega)]$ in the

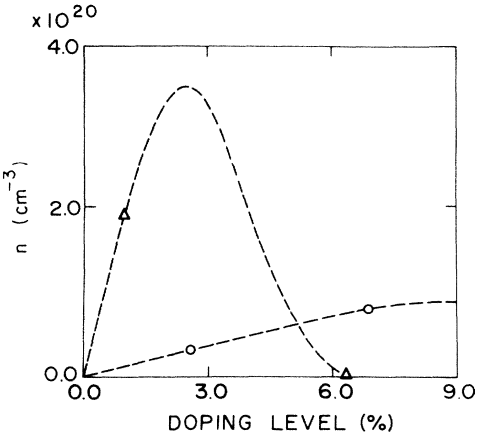

FIG. 8. Comparison of the integrated oscillator strength of the soliton lattice and the polaronlike lattice. The open circles refer to the soliton lattice, and the open triangles to the polaron lattice.

various structural distortions. As we track the integrated oscillator strength in the spectra (shown in Fig. 8) calculated for the soliton lattice, the integrated strength tracks roughly linearly with dopant density for low concentration, becoming sublinear as the solitons overlap above $\rho=4\%$. The integrated oscillator strength for the polaronlike lattice is larger than that for the soliton lattice by the factor of 10 at small density. In Horvitz's theory[4] this is attributable to the small inertial mass of the polaron relative to the soliton. However, this decreases much more rapidly as dopant density increases. By 6% the integrated strength nearly vanishes for the polaronlike lattice. This result occurs as the amplitude of the order parameter is suppressed at high concentration. This result makes sense in the limit of the undimerized lattice [$\Delta(x)=0$], for which we can prove that $j_d(x)=0$ as follows. If the order parameter has even parity or $\Delta(-x)=\Delta(x)$, as is the case with the polaronlike lattice, then it follows from the fact that the dynamical charge has the opposite parity to the structural distortion, that $j_d(-x)=-j_d(x)$. However, if $\Delta(-x)=-\Delta(x)$, then it follows that $j_d(-x)=j_d(x)$. Therefore, for the undimerized lattice of $\Delta(x)=0$, which satisfies both $\Delta(-x)=\Delta(x)$ and $\Delta(-x)=-\Delta(x)$, we have $j_d(x)=0$. The polaronlike lattice at high density has a very small structural distoration, i.e., $\Delta(x)=0$ is roughly satisfied. This rationalizes the small oscillator strength of polaronlike lattice at high density.

In summary, the main differences between the soliton lattice absorption spectra and the polaronlike lattice absorption spectra are, first of all, the difference in the magnitude of absorption spectra; at low density the magnitude of polaronlike lattice is larger by a factor of 10, and at high density, the polaronlike lattice has a vanishingly small strength. Secondly, the polaronlike lattice has more fine structure than the soliton lattice, and finally the polaronlike lattice will have a stronger (though broader) absorption spectra around $\omega=0$ than the soliton lattice due to the electronic intraband transition.

IV. CONCLUSION

We have studied a continuum model of a coupled electron-phonon system in polyacetylene including the coupling of several relevant structural degrees of freedom to the π-electron density, to calculate the phonon-assisted absorption spectra. Our results show that there are two ir-active modes for the soliton lattice and the absorption spectra for it look similar to those for the single polaron calculated by several groups.[10] The polaronlike lattice has more fine structure in the absorption spectra than those of soliton latttice at 1—4% density and has vanishingly small oscillator strength at $\geq 6\%$ density, which is not consistent with the experiments. It is found experimentally that the oscillator strength is roughly proportional to the doping density, and that the absorption spectra does not have much structure in addition to the T modes. As expected, the crossover from soliton lattice to polaronlike distortion is not found in our strictly one-dimensional calculation. Moreover, it should be noted that the polaronlike distortion at high doping density is unstable against the undimerized lattice (even in the presence of Coulomb interaction with dopant ions), which causes the oscillator strength of polaronlike lattice to be very small. Since experiments, as noted above, do not show this behavior, there still remains the question of what derives the abrupt onset of Pauli magnetic sucseptibility while the electric conductivity remains roughly the same. There was a proposition that this might be caused by the disorder induced by the doping procedure.[16] Some interactions neglected in the Su-Schrieffer-Heeger or TLM Hamiltonian such as three-dimensional interaction and electron-electron Coulomb repulsion might be important at this point. Among these, we think that the commensurability effect in the discrete Hamiltonian may play an important role. Once the system has been brought to the continuum limit, the possible locking with other commensurabilities like the $\frac{5}{9}$, $\frac{4}{7}$, $\frac{3}{5}$, . . .-filled band has been removed. We believe that the description in terms of soliton lattice is good provided that the deviation from the commensurability $\frac{1}{2}$ (half-filled band) is small, but that if the deviation gets larger the possibility of locking into another commensurate value might play an important role. We are currently studying this problem.

ACKNOWLEDGMENTS

This work was supported by NSF through Grant No. DMR 84-05524. E.J.M. gratefully acknowledges additional support from Alfred P. Sloan Foundation.

[1]W. P. Su, J. R. Schrieffer, and A. J. Heeger, Phys. Rev. Lett. **42**, 1698 (1979); Phys. Rev. B **22**, 2209 (1980); **28**, 1138(E) (1983).
[2]J. Chen, T. C. Chung, F. Moraes, and A. J. Heeger, Solid State Commun. **53**, 757 (1985).
[3]S. Kivelson and A. J. Heeger, Phys. Rev. Lett. **55**, 308 (1985).
[4]B. Horovitz, Phys. Rev. Lett. **46**, 742 (1981); S. A. Brazovskii, S. A. Gordyunin, and N. N. Kirova, Pis'ma Zh. Eksp. Teor. Fiz. **31**, 486 (1980) [JETP Lett. **13**, 456 (1980)].
[5]H. Takayama, Y. R. Lin Liu, and K. Maki, Phys. Rev. B **21**, 2388 (1980).
[6]H. Ito, A. Terai, Y. Ono, and Y. Wada, J. Phys. Soc. Jpn. **53**, 3520 (1984).
[7]A. Terai, H. Ito, Y. Ono, and Y. Wada, J. Phys. Soc. Jpn. **54**, 196 (1985).
[8]J. C. Hicks and G. A. Blaisdell, Phys. Rev. B **31**, 919 (1985).
[9]H. Y. Choi and E. J. Mele (unpublished).
[10]E. J. Mele and J. C. Hicks, Phys. Rev. B **32**, 2703 (1985).
[11]H. Ito and Y. Ono, J. Phys. Soc. Jpn. **54**, 1194 (1985).
[12]B. Horovitz, Solid State Commun. **41**, 729 (1982).
[13]B. Horovitz, Z. Vardeny, E. Ehrenfreund, and O. Brafman, Synth. Metals **9**, 215 (1984).
[14]Z. Vardeny, E. Ehrenfreund, O. Brafman, J. Tanaka, H. Fujimoto, and M. Tanaka (unpublished).
[15]J. C. Hicks and J. T. Gammel, Phys. Rev. Lett. **57**, 1320 (1986).
[16]E. J. Mele and M. J. Rice, Phys. Rev. B **23**, 5397 (1981).